Journal of ELECTRONIC MATERIALS, Vol. 49, No. 9, 2020
https://doi.org/10.1007/s11664-020-08211-w
© 2020 The Minerals, Metals & Materials Society

TOPICAL COLLECTION: 18TH CONFERENCE ON DEFECTS (DRIP XVIII)

Photoelastic Characterization of Residual Strain Distribution in Commercial Off-Axis SiC Substrates

MASAYUKI FUKUZAWA [1,2] and KAZUKI KANAMOTO [1]

1.—Graduation School of Science and Technology, Kyoto Institute of Technology, Kyoto 606-8585, Japan. 2.—e-mail: fukuzawa@kit.ac.jp

Two-dimensional distribution of strain-induced birefringence has been selectively characterized in commercial 4° off-axis wafers of 4H-silicon carbide (SiC) crystal by using an originally-developed imaging polariscope. The natural birefringence, which is often observed in uniaxial crystals, was eliminated by optimizing the light incident angle so that the light propagates parallel to the *c*-axis inside the crystal. The eliminated natural birefringence was at least twice as large as that of the strain-induced ones, which demonstrates the validity of the elimination process. A typical retardation map under optimal incidence revealed various distributions of strain-induced birefringence, such as local concentrations due to the structural crystal defects and gradual increase or relief due to the thermal stress during the crystal growth and cooling processes. The maximum retardation was 0.28, which corresponds to 7.6×10^{-5} in strain terms, and 30 MPa in stress terms. Because of its sufficient sensitivity to the strain-induced birefringence and elimination capability in the natural birefringence, it is concluded that our technique is useful to characterize the residual strain distribution in commercial off-axis SiC substrates.

Key words: SiC, residual strain, photoelastic characterization, off-axis substrate

INTRODUCTION

Silicon carbide (SiC) is a promising material for substrates of various power devices due to its superior electrical and thermal properties.[1–3] There is a strong demand for commercial substrates of large diameter wafers with homogeneous properties, not only to increase the device productivity but also to enlarge the die size for a high current rating. However, commercial SiC crystals, which are mainly grown by a sublimation technique, still include structural crystal defects in various shapes and sizes, such as basal plane dislocation, threading edge and screw dislocations, micropipes, and subgrain boundaries.[1,2] Since such structural defects are unevenly distributed and sometimes concentrated locally in the wafer, they act as local plastic deformation and partly relieve the thermal stresses inhomogeneously during the crystal growth and consequent cooling processes. In this case, a part of the unrelieved thermal stresses are locally frozen in the crystal as residual strain or stress after the cooling processes to keep the local force balance. The residual strain or stress in the wafer may cause unwanted issues during the device fabrication process, such as defect propagation, cracks, and breakage. Therefore, it is important to examine the residual strain distribution in commercial SiC wafers.

In order to characterize the residual strain in various semiconductor crystals, we developed a scanning infrared polariscope[4] and several imaging polariscopes.[5,6] These polariscopes were specialized for a thin ($\sim$ mm) semiconductor wafer as a

(Received December 17, 2019; accepted May 8, 2020; published online May 20, 2020)

birefringent plate to obtain the two-dimensional distribution of principal in-plane strain components normal to the incident light by measuring the phase retardation δ and principal direction ψ of birefringence if there is no natural birefringence and the photoelastic constants are known. By using these polariscopes, we have successfully examined the two-dimensional distribution of residual strain in several commercial wafers, such as GaAs, GaP, InP, Si, mc-Si, and GaN.[4–9] However, we did not examine off-axis SiC wafers because of their natural birefringence.

In this study, we examined residual strain distribution in commercial off-axis SiC wafers. A simple technique is proposed to eliminate the natural birefringence by optimizing the light incident angle. The effectiveness and significance of this technique is demonstrated by comparing the magnitude of strain-induced birefringence and natural birefringence examined in commercial 4-inch (c. 10-cm) 4H-SiC 4° off-axis wafers. A typical retardation map under the optimal incident angle is presented to discuss typical strain distributions and their primary origins. In order to clarify the features and advantages of our technique, it is also compared with the crossed-Nicols image which is known as a conventional technique for the observation of crystal defects in SiC wafers.

METHOD FOR SELECTIVE MEASUREMENT OF STRAIN-INDUCED BIREFRINGENCE

SiC and other hexagonal crystals are uniaxial and often reveal natural birefringence as well as strain-induced ones due to photoelastic effects. Therefore, any effect of natural birefringence should be eliminated for characterizing the residual strain in SiC crystals. The natural birefringence is easily eliminated in the case of "just" c-plane wafers by normal incidence of the light to the wafer surface, because the natural birefringence is not revealed when the light is propagated parallel to the *c*-axis. On the other hand, it is not easy in the case of off-axis wafers because the incident angle should be optimized so that the light propagates to the *c*-axis inside the crystal.

Figure 1 shows a simple sketch of light-propagation in an off-axis substrate. We assume a substrate with an off-angle θ_{off} and a collimated light introduced to the substrate with an incident angle θ_{b}. The light propagation is described by Snell's law, as in Eq. 1:

$$\sin\theta_b = \frac{n_{\mathrm{S}}}{n_{\mathrm{A}}}\sin\left(\theta_{\mathrm{off}} + \theta_{\mathrm{p}}\right) \tag{1}$$

where θ_{p} is the light-propagation angle with respect to the *c*-axis, n_{A} and n_{S} are refractive indices of air and the substrates, respectively. An optimized incident angle is easily determined by assuming θ_{p} is zero.

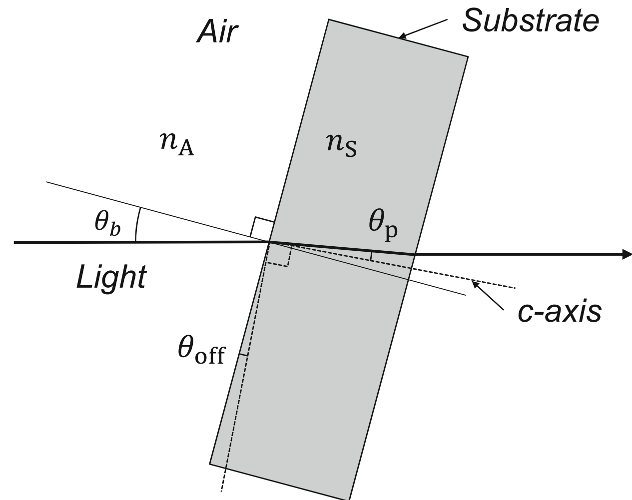

Fig. 1. Sketch of light propagation in an off-axis substrate.

In this study, a motorized rotation stage was added to the near-infrared imaging polariscope (NIRIP),[5] and its control software was modified to measure retardation maps by tilting the substrate to adjust θ_b according to θ_{p} which had been specified by user as arbitrary parameter in advance. Figure 2 shows its functional block diagram. If n_{S} and θ_{off} are well known, a retardation map without natural birefringence can be automatically obtained by simply specifying $\theta_{\mathrm{p}} = 0$. A series of retardation maps can also be automatically obtained by specifying a value list of θ_{p}, including any non-zero values, which is effective for examining the θ_{p} dependence on the retardation map for validating the n_{S} and θ_{off}.

In uniaxial crystals such as SiC, the strain component in the c-plane is related to the retardation, as in Eq. 2.[10]

$$|S_1 - S_2| = \frac{\lambda\delta}{\pi d n_0^3 (p_{11} - p_{12})} \tag{2}$$

where S_1 and S_2 are strain components along the principal directions, λ is the wavelength of the polarized incident light, d is the thickness of the substrate, n_0 is the refractive index of the unstrained substrate, and $(p_{11} - p_{12})$ is the photoelastic coefficient.

The substrates used in this study are commercially-available 4-inch (c. 10-cm) 4° off-axis wafers of 4H SiC crystal grown by a sublimation technique. The level of etch pit density (EPD) was 5×10^3 cm^{-2}. An old 3-inch (c.7.6-cm) 6H SiC wafer was also examined for comparison. It has an order of magnitude higher EPD than that of the 4-inch (c. 10-cm) wafers and it also includes many structural crystal defects large enough to be visible to the naked eye. In this study, we used the nominal value

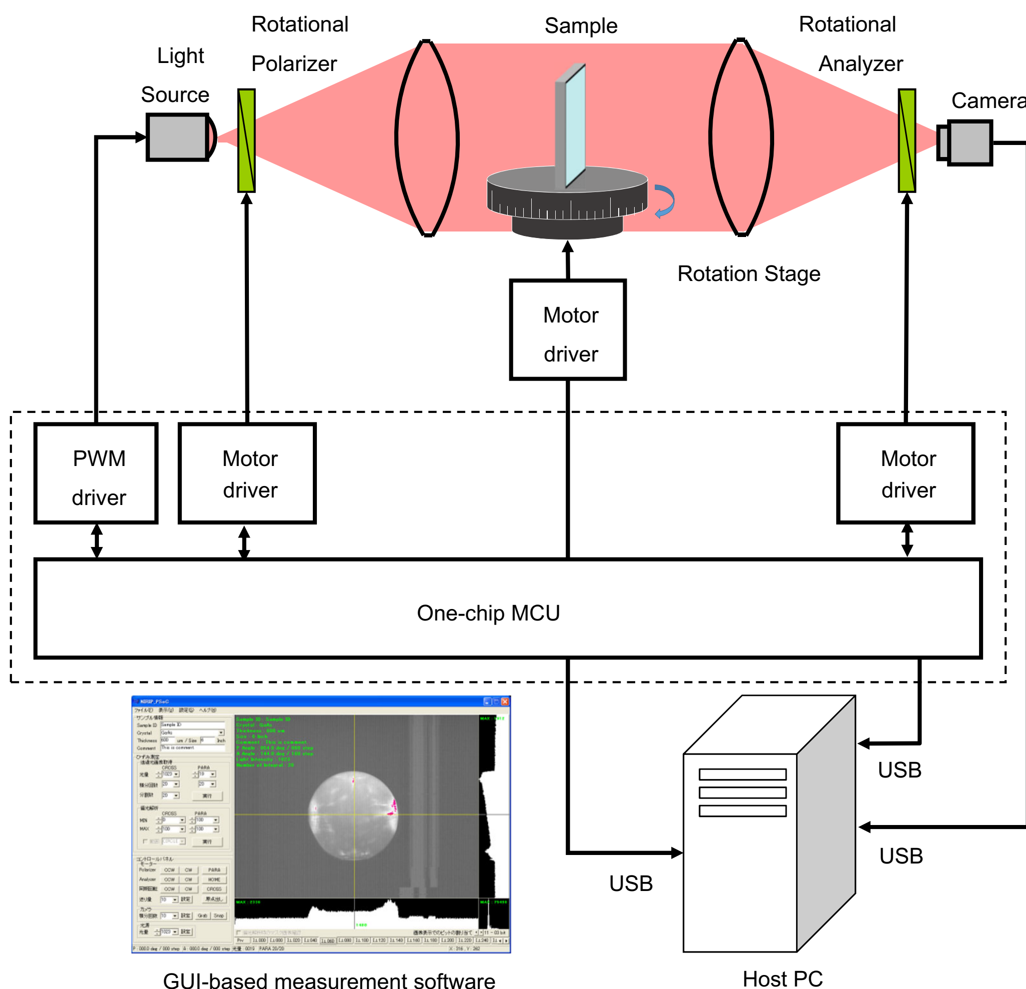

Fig. 2. Functional block diagram of the imaging polariscope with a motorized rotation stage.

of $\theta_{\rm off} = 4°$ from the wafer specification sheets, the literature values for $c_{\rm ij}$,[11] a calculated value of $n_{\rm S}$ at λ = 940 nm from a temperature-dependent Sellmeier equation,[12] and an experimental value of 0.12 for $(p_{11} - p_{12})$ obtained from a simple load test by ourselves, whose details will be published elsewhere.

RESULTS AND DISCUSSIONS

Figure 3 shows a series of retardation maps of a typical 4-inch (c. 10-cm) 4H-SiC 4° off-axis wafer measured with several $\theta_{\rm p}$ to examine their dependence. The condition of $\theta_{\rm p} = 0$ represents a theoretically-expected optimal incidence ($\theta_{\rm b} \neq 0$) where the natural birefringence is eliminated, and that of $\theta_{\rm p} = -4°$ means the conventional normal incidence to the substrate surface ($\theta_{\rm b} = 0$). The average of retardation over a whole wafer μ_δ was also calculated for each map, as shown in Fig. 4. It clearly revealed strong and symmetrical variation around $\theta_{\rm p} = 0$, which agrees with the theory. Therefore, it can be confirmed that the values of $n_{\rm S}$ and $\theta_{\rm off}$ were accurate enough to give an optimal $\theta_{\rm b}$ at $\theta_{\rm p} = 0$. The magnitude of μ_δ at $\theta_{\rm p} = 0$ was one-third as large as that at $\theta_{\rm p} = -4°$. This means that the contribution of natural birefringence was at least twice as large as that of strain-induced ones under the normal incident condition in this wafer. Although that contribution ratio may vary from wafer to wafer, this fact demonstrates the validity of the elimination process in the residual strain characterization of off-axis SiC wafers. Inevitably, the normal incident condition may mislead the interpretation of the retardation maps.

The spatial fluctuation was clearly recognized mainly in the retardation maps with small $\theta_{\rm p}$ rather than that with large $\theta_{\rm p}$. The standard deviation of the retardation over the whole wafer σ_δ was about 14% of μ_δ at $\theta_{\rm p} = 0$, while it was 7% at $\theta_{\rm p} = -4°$. It is well known that strain-induced birefringence is mostly distributed inhomogeneously due to local concentrations of crystal defects or thermal stresses, while the natural birefringence is almost homogeneously distributed unless the stoichiometric composition is varied or the crystal orientation is rotated. Therefore, it is reasonable to interpret that

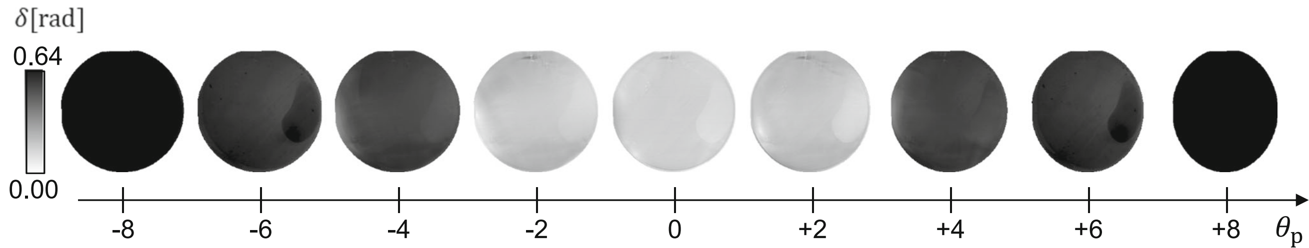

Fig. 3. Retardation maps of a commercially-available 4-inch (c. 10-cm) 4H-SiC 4° off-axis wafer with several light-propagation angles, θ_p, with respect to the *c*-axis.

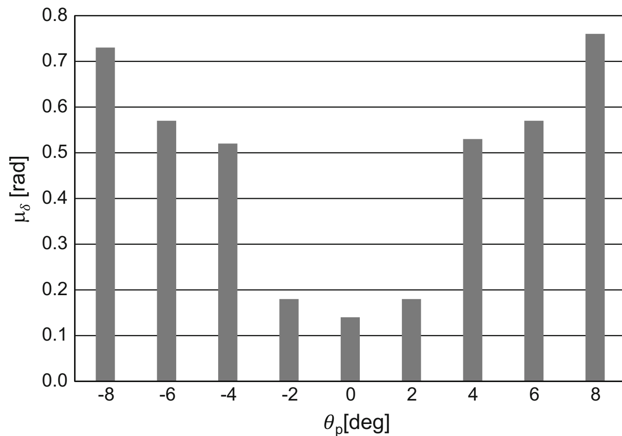

Fig. 4. The retardation average over a whole wafer μ_δ calculated for each retardation map.

the homogeneous natural birefringence was eliminated and the inhomogeneous strain-induced birefringence became dominant in the retardation maps with small θ_p. Thus, we characterize the residual strain distribution with the retardation map measured under the optimal incidence.

Figure 5 shows the retardation maps measured under the optimal incidence in (a) the same wafer shown in Fig. 3 and (b) an old 3-inch (c. 7.6-cm) 6H-SiC wafer for comparison. It is noted that the δ scale was individually determined based on its maximum δ values to optimize the contrast for each map. The maximum δ values of (a) and (b) were 0.28 and 0.93 and they correspond to 7.6×10^{-5} and 2.5×10^{-4} in strain terms and 30 MPa and 98 MPa in stress terms, respectively. The maximum δ value of (b) was more than three times as large as that of (a), and both μ_δ and σ_δ of (b) were around twice as large as those of (a), which may reflect a high dislocation density and a large number of structural crystal defects in the old 3-inch (c. 7.6-cm) wafer. Various types of strain distribution were clearly found in both wafers, whose typical areas are indicated by ovals noted as a_1, a_2, a_3, a_4, b_1, and b_2. Figure 6 shows the transmission x-ray topography images of two small areas, X_1 and X_2, in an adjacent wafer to that shown in Fig. 5, where the corresponding areas are indicated as dashed rectangles. The topography image X_1 clearly revealed a large and complicated structure of crystal defects distributed from the upper center to the lower right of the area. Such structural defects must be commonly found even in the adjacent wafers because their distribution area is much wider than the wafer thickness. On the other hand, they were not found in the area X_2 except for the weak inhomogeneity of fine crystal defects.

One typical strain distribution is "local concentrations" inside the wafer, which were found in the areas a_1 and b_1. The area a_1 is a slightly apart from the orientation flat and includes a simple strain concentration in the shape of a thick horizontal filament. Since it is solely and locally concentrated and has a clear boundary, it must be due to structural crystal defects generated unevenly in some local regions of the wafer. The existence of the large structural defects in the topography image X_1 supports that speculation. It should be noted here that the defect distribution itself was significantly different from the strain distribution. The area b_1 revealed more complicated shapes of many thin filaments, which clearly reflect a high-density of structural crystal defects.

Another typical strain distribution is a "gradual increase or relief" toward the wafer edge around certain directions. The areas a_2, and a_4 included gradual strain increases and a_3 had relief toward the wafer edge. The regions are alternatively located and spread and have no clear boundaries. Such wide and gradual strain distribution must be related mainly to the thermal stress distribution during the crystal growth or cooling processes because of their locality. The topography image X_2 supports this speculation because there are no structural crystal defects except for the weak inhomogeneity of fine defects. However, the defect distribution itself was also different from the strain distribution. The area b_2 revealed the gradual strain increase as found in a_2 and a_4 but also included the local strain fluctuation in a complicated shape as in b_1.

We examined many commercial off-axis SiC wafers and confirmed that those strain distributions mentioned above were commonly found, but their appearance frequency and place strongly varied between each other. It was also confirmed that in most cases the defect distribution was apparently

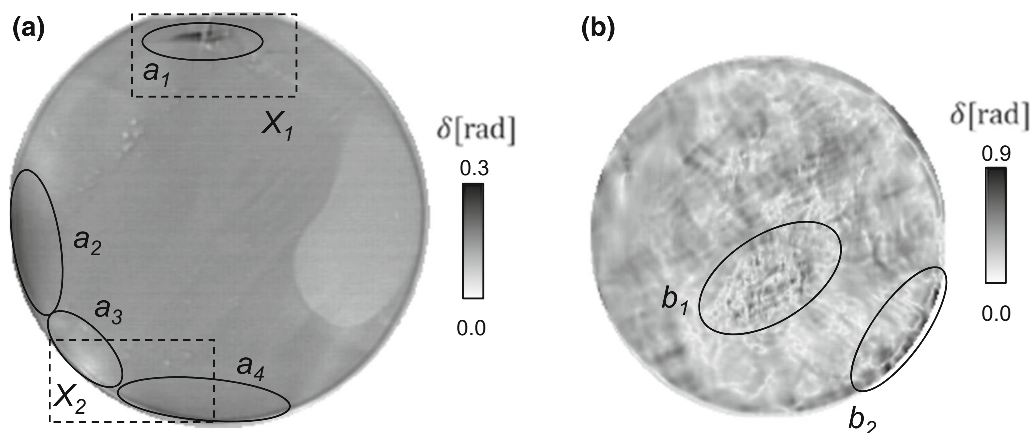

Fig. 5. Retardation maps at $\theta_p = 0$ in (a) the wafer shown in Fig. 3 and (b) a 3-inch (c. 7.6-cm) 6H-SiC wafer.

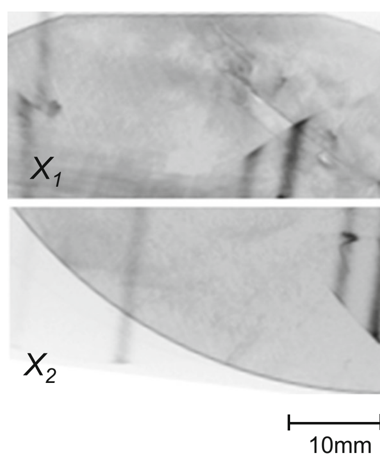

Fig. 6. Transmission x-ray topography images obtained in two small areas X_1 and X_2 of an adjacent wafer to that shown in Fig. 3.

different from the strain distribution, which may imply that our photoelastic technique and transmission x-ray topography are not alternates but complementary. Since a certain part of those strain distributions may cause unwanted issues during the device fabrication processes, it is valuable to examine the commercial off-axis SiC wafers in different batches.

An essential difference between the conventional crossed-Nicols image and our polariscope is the sensitivity-dependence on the strain direction. The crossed-Nicols image is widely used to observe structural crystal defects such as micropipes. However, it is sensitive only to the strain components perpendicular to the polarization direction. Therefore, the crossed-Nicols image does not agree with the residual strain distribution even if the natural birefringence would somehow be eliminated. On the other hand, our polariscope is sensitive to the strain components of all directions because it has a function of a complete ellipsometer with a single wavelength. Thus, we can quantitatively characterize the residual strain distribution in the commercial off-axis SiC wafers only if the natural birefringence is eliminated by the technique shown in this study. This must be useful for the quality assessment of SiC wafers, especially large-diameter ones.

CONCLUSIONS

Residual strain distribution has been selectively characterized in commercial 4-inch (c. 10-cm) 4H-SiC 4° off-axis wafers with an improved version of the NIRIP. The natural birefringence was eliminated by optimizing the light incident angle so that the light propagates parallel to the *c*-axis inside the crystal. The amount of eliminated natural birefringence was at least twice as large as that of strain-induced ones, which demonstrates the validity of the elimination process. Under the optimal incident angle, a typical retardation map revealed its maximum values as 0.28 which corresponds to 7.6×10^{-5} in strain terms and 30 MPa in stress terms. The retardation maps of many off-axis SiC wafers commonly revealed typical strain distributions, such as local concentrations due to the structural crystal defects and gradual increase or relief due to the thermal stress during the crystal growth and/or cooling processes, but their appearance frequency and place strongly varied between each other. Since our technique has sufficient sensitivity to the strain-induced birefringence and elimination capability in the natural birefringence, we can conclude that it is useful for characterizing the residual strain distribution in commercial off-axis SiC substrates.

ACKNOWLEDGMENT

This work was supported by JSPS KAKENHI Grant Number JP17K05040.

REFERENCES

1. T. Kimoto and J.A. Cooper, *Fundamentals of Silicon Carbide Technology* (Hoboken: Wiley-IEEE, 2014).
2. P. Friedrichs, T. Kimoto, L. Ley, and G. Pensl, eds., *Silicon Carbide*, Vol. 1 (Hoboken: Wiley-VCH, 2009).

3. P. Friedrichs, T. Kimoto, L. Ley, and G. Pensl, eds., *Silicon Carbide*, Vol. 2 (Hoboken: Wiley-VCH, 2009).
4. M. Yamada, K. Ito, and M. Fukuzawa, in *Proceedings of SIMC-9* (1996), pp. 177–180.
5. M. Fukuzawa and M. Yamada, *Phys. Status Solidi (c)* 5, 2941–2943 (2008).
6. M. Fukuzawa and M. Yamada, in *Proceedings of IPRM2008* (2008), TuB.1-1-Inv.
7. M. Fukuzawa and M. Yamada, *J. Cryst. Growth* 229, 22–25 (2001).
8. K. Jiptner, B. Gao, H. Harada, Y. Miyamura, M. Fukuzawa, K. Kakimoto, and T. Sekiguchi, *J. Cryst. Growth* 408, 19–24 (2014).
9. M. Fukuzawa, R. Kashiwagi and M. Yamada, in *Proceedings of IPRM2010* (2010), pp. 184–186.
10. J.F. Nye, *Physical Properties of Crystals* (London: Oxford Unversity Press, 1957).
11. K. Kamitani, M. Grimsditch, J.C. Nipko, and C.-K. Loong, *J. Appl. Phys.* 82, 3152 (1997).
12. C. Xu, S. Wang, G. Wang, J. Liang, S. Wang, L. Bai, J. Yang, and X. Chen, *J. Appl. Phys.* 115, 113501 (2014).

Publisher's Note Springer Nature remains neutral with regard to jurisdictional claims in published maps and institutional affiliations.